

Article

Comparative Study of the Compressibility of $M_3V_2O_8$ (M = Cd, Zn, Mg, Ni) Orthovanadates

Daniel Díaz-Anichtchenko and Daniel Errandonea * 

Departamento de Física Aplicada-ICMUV, MALTA Consolider Team, Universitat de València, Dr. Moliner 50, 46100 Burjassot, Spain

* Correspondence: daniel.errandonea@uv.es

Abstract: We report herein a theoretical study of the high-pressure compressibility of $Cd_3V_2O_8$, $Zn_3V_2O_8$, $Mg_3V_2O_8$, and $Ni_3V_2O_8$. For $Cd_3V_2O_8$, we also present a study of its structural stability. Computer simulations were performed by means of first-principles methods using the CRYSTAL program. In $Cd_3V_2O_8$, we found a previously unreported polymorph which is thermodynamically more stable than the already known polymorph. We also determined the compressibility of all compounds and evaluated the different contributions of polyhedral units to compressibility. We found that the studied vanadates have an anisotropic response to compression and that the change in volume is basically determined by the compressibility of the divalent-cation coordination polyhedra. A systematic discussion of the bulk modulus of $M_3V_2O_8$ orthovanadates will also be included.

Keywords: high pressure; vanadates; bulk modulus; anisotropy



Citation: Díaz-Anichtchenko, D.; Errandonea, D. Comparative Study of the Compressibility of $M_3V_2O_8$ (M = Cd, Zn, Mg, Ni) Orthovanadates. *Crystals* **2022**, *12*, 1544. <https://doi.org/10.3390/cryst12111544>

Academic Editors: Pier Carlo Ricci, Simone Anzellini, Anna Herlihy and Robin Turnbull

Received: 14 October 2022

Accepted: 26 October 2022

Published: 28 October 2022

Publisher's Note: MDPI stays neutral with regard to jurisdictional claims in published maps and institutional affiliations.



Copyright: © 2022 by the authors. Licensee MDPI, Basel, Switzerland. This article is an open access article distributed under the terms and conditions of the Creative Commons Attribution (CC BY) license (<https://creativecommons.org/licenses/by/4.0/>).

1. Introduction

In modern society, every day the need for less contaminated and more energy efficient materials is more evident. Complex vanadium materials have received a great deal of attention for developing green technologies. Nowadays, they are being considered as electrodes for rechargeable batteries and as photocatalytic materials [1–6]. Orthovanadates, with formula $M_3V_2O_8$, being M a divalent atom, are also interesting because of their optical, dielectric, and magnetic properties [7–10]. On top of that, these materials have received a great deal of attention owing to their luminescence properties [11], which make them promising materials as laser-host matrices and for developing light-emitting diodes [12]. In addition, $M_3V_2O_8$ vanadates have attracted attention because of their self-activated photoluminescence [13]. Interestingly, the colors of their photoluminescence cover almost the whole visible-light region from blue to yellow.

From the fundamental point of view, the high-pressure (HP) behavior of $M_3V_2O_8$ vanadates has also been the focus of recent studies [14–16]. X-ray diffraction experiments have shown that $Zn_3V_2O_8$ [14] and $Ni_3V_2O_8$ [15] remain stable in the low-pressure phase up to 15 GPa. In $Mn_3V_2O_8$ [16], the onset of a structural phase transition has been located beyond 10 GPa. On the other hand, the bulk moduli of $M_3V_2O_8$ vanadates have been determined to cover a range of values from 100 GPa to 140 GPa. However, a systematic understanding of this physical parameter has not been established yet. On top of that, there are materials such as $Mg_3V_2O_8$ and $Cd_3V_2O_8$ which have never been studied under high-pressure conditions.

Here, we report a study of the compressibility of $Zn_3V_2O_8$, $Ni_3V_2O_8$, $Mg_3V_2O_8$, and $Cd_3V_2O_8$ and of the HP structural stability of $Cd_3V_2O_8$. To achieve our goals, we have performed density-functional theory (DFT) calculations. This method has been proven to provide an efficient framework to study the behavior under pressure of materials including ternary oxides [17–20]. The obtained results have been validated by a comparison with experiments. We have found that the volume change under HP is mainly due to the volume

decrease in MO_6 octahedral units. We also found evidence supporting the existence in $\text{Cd}_3\text{V}_2\text{O}_8$ of a previously unreported polymorph.

2. Computational Details

First-principles total-energy calculations were performed within the periodic DFT framework using the CRYSTAL14 program package [21]. The exchange correlation functionals were described using three different approximations: Becke–Lee–Yang–Parr (B3LYP) [22,23] and Heyd–Scuseria–Ernzerhof (HSE06) [24] hybrid functionals, and Perdew–Burke–Ernzerhof (PBE) standard functionals [25]. The electron basis sets employed to describe Cd, Ni, Zn, Mg, V, and O atoms were taken from the Crystal website [26]. Using the Pack–Monkhorst/Gilat shrinking factors $IS = ISP = 4$ we have controlled the diagonalization of the Fock matrix. This procedure was carried out using adequate fine grids of irreducible k-points in the reciprocal space. The TOLINTEG parameters, controlling the tolerance factors for the Coulomb and exchange integrals, were set to 10^{-14} to assure a convergence in total energy that is more accurate than 10^{-7} Hartree. Relative numerical errors in the determination of unit-cell parameters are smaller than 10^{-4} . The percent of Fock/Kohn–Sham matrices mixing was set to 40. The choice of the exchange–correlation functional is of critical importance as it has a significant influence on the description of physical properties [27]. Based upon our previous work in related $\text{Zn}_2\text{V}_2\text{O}_7$ [28] and $\text{Cd}_2\text{V}_2\text{O}_7$ [29], and on the fact that in the present calculations we found that B3LYP better describes the structures of all studied compounds at ambient pressure, we employed only B3LYP functionals for present high-pressure studies. Since computer simulations have been performed with the intention of comparing the results among the studied materials at room-temperature, in which $\text{Ni}_3\text{V}_2\text{O}_8$ is paramagnetic, calculations for this compound were performed only for the paramagnetic configuration. To consider long-range Van der Waals interactions, we included them in calculations using the semi-empirical contributions proposed by Grimme [30], which are especially useful to give an accurate description for metal oxides. All the calculated structures are dynamically stable, having real frequencies over the full Brillouin Zone. From total-energy calculations, the pressure (P)–volume (V) relationship was calculated from the energy (E) versus volume (V) curves. The enthalpy (H) of different polymorphs was determined using $H = E + P \times V$. Crystal structures were represented using VESTA [31], which was also used to calculate polyhedral volumes.

3. Results and Discussion

3.1. Crystal Structure

The crystal structures of $\text{Zn}_3\text{V}_2\text{O}_8$, $\text{Mg}_3\text{V}_2\text{O}_8$, and $\text{Ni}_3\text{V}_2\text{O}_8$ are isomorphic. Their prototypic structure (also shared by $\text{Co}_3\text{V}_2\text{O}_8$ and $\text{Mn}_3\text{V}_2\text{O}_8$) is described by the orthorhombic space group $Cmca$ and has four formula units per unit-cell [32–34]. This orthorhombic structure is represented in Figure 1a. It is formed by edge-sharing MO_6 ($M = \text{Mg}, \text{Ni}, \text{Zn}$) octahedra forming two-dimensional Kagome-type staircases which are separated by VO_4 isolated tetrahedra which corner-shared oxygen atoms with the MnO_6 octahedra.

The crystal structure of $\text{Cd}_3\text{V}_2\text{O}_8$ is also orthorhombic. A schematic representation of it is shown in Figure 1b. The structure has been described in the literature by space group $Pnma$ and has two formula units per unit cell [35]. However, in this description, there is one 4c Wyckoff position occupied by Cd atoms with an occupation factor equal to 1/2. We found that if the structure is described instead by orthorhombic space group $Pmc2_1$ (a subgroup of $Pnma$) the 4c Wyckoff position of Cd splits in to one 2a and one 2b Wyckoff positions. Assuming that Cd atoms are at 2a sites and 2b sites are vacant, an equivalent crystal structure is obtained. However, in this case, all atomic positions have a structural occupation factor equal to 1. Both descriptions give identical X-ray diffraction patterns and can be used to describe the structure of $\text{Cd}_3\text{V}_2\text{O}_8$. Nevertheless, the second one (space group $Pmc2_1$) is the most convenient for calculations. Consequently, when describing $\text{Cd}_3\text{V}_2\text{O}_8$ in this work, we will use space group $Pmc2_1$. As shown in Figure 1b, the structure of cadmium orthovanadate is composed by CdO_6 octahedra that share edges

forming chains in the [100] direction separated by a chain of alternating CdO_4 and VO_4 tetrahedral units.

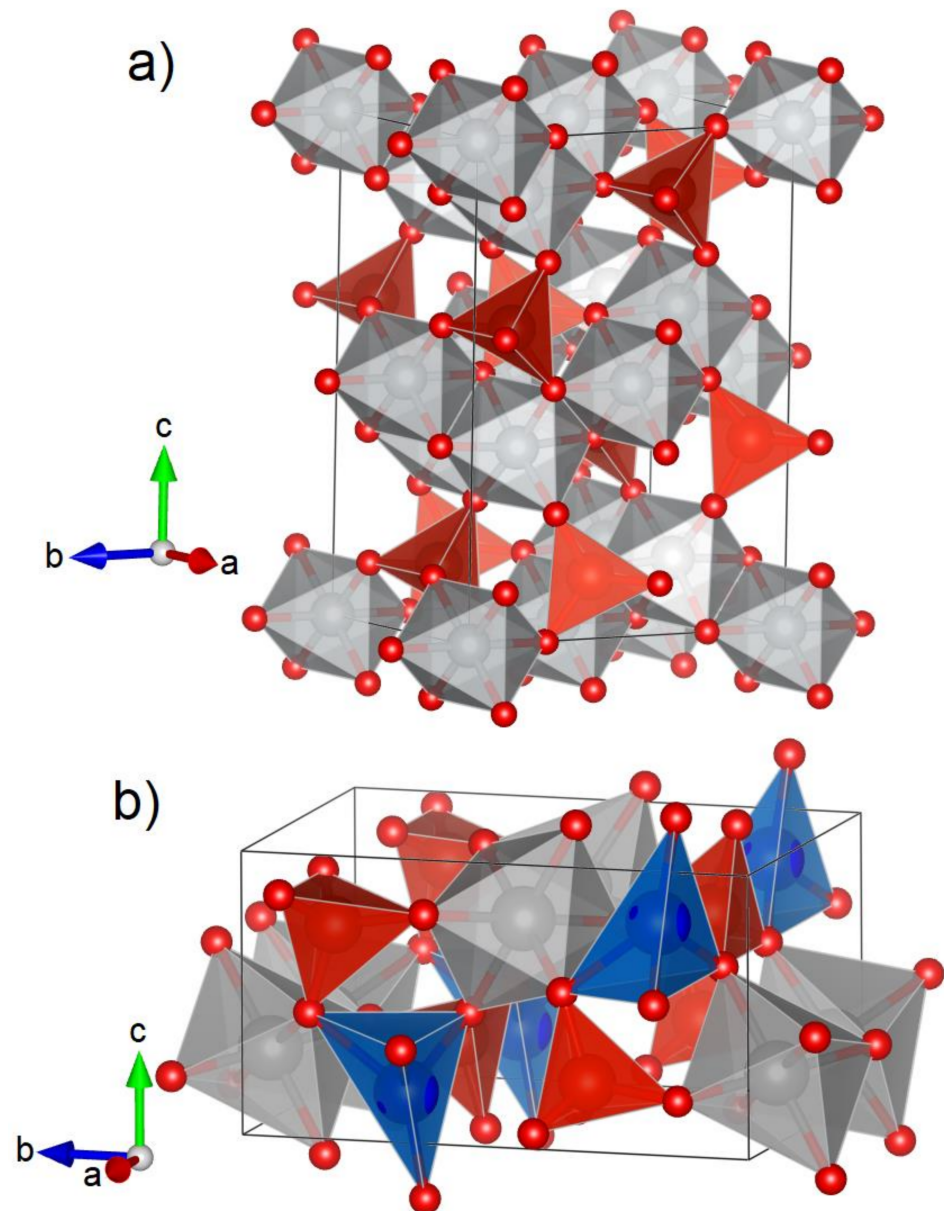


Figure 1. (a) Schematic representation of the crystal structure of $\text{Ni}_3\text{V}_2\text{O}_8$ and isomorphous $\text{M}_3\text{V}_2\text{O}_8$ compounds. MO_6 octahedra are shown in gray and VO_4 tetrahedra in red. Red circles represent the oxygen atoms. (b) Schematic representation of the crystal structure of $\beta\text{-Cd}_3\text{V}_2\text{O}_8$ using space group $Pmc2_1$. CdO_6 octahedra are shown in gray, CdO_4 tetrahedra in blue, and VO_4 tetrahedra in red. Red circles represent the oxygen atoms.

In our study, we have also considered a second possible polymorph for $\text{Cd}_3\text{V}_2\text{O}_8$ which we assumed was isomorphous to $\text{Zn}_3\text{V}_2\text{O}_8$, $\text{Mg}_3\text{V}_2\text{O}_8$, and $\text{Ni}_3\text{V}_2\text{O}_8$. We will name it $\alpha\text{-Cd}_3\text{V}_2\text{O}_8$ (to use the same name used in the literature for the isomorphous vanadates), and we will name the polymorph previously reported in the literature (described by space group $Pmc2_1$) as $\beta\text{-Cd}_3\text{V}_2\text{O}_8$. Interestingly, our calculations found that $\alpha\text{-Cd}_3\text{V}_2\text{O}_8$ has a lower enthalpy than $\beta\text{-Cd}_3\text{V}_2\text{O}_8$ from ambient pressure up to 14 GPa (see Figure 2), with the enthalpy difference increasing as pressure increases. This result means that $\alpha\text{-Cd}_3\text{V}_2\text{O}_8$ is thermodynamically more stable. This means that it might be synthesized at ambient conditions using a different synthesis route than that used by Ben Yahia et al. [35]

or the β - α phase transition could be driven by relatively low pressures at room temperature. The fact that the volume per formula unit of α - $\text{Cd}_3\text{V}_2\text{O}_8$ (168.1 \AA^3) is 6% smaller than the volume per formula unit of β - $\text{Cd}_3\text{V}_2\text{O}_8$ (178.5 \AA^3) is consistent with the second hypothesis. The calculated atomic positions of α - $\text{Cd}_3\text{V}_2\text{O}_8$ are given in Table 1. Its unit-cell parameters can be found in Table 2.

The unit-cell parameters of the crystal structures optimized for all studied compounds at zero pressure using B3LYP functionals are provided in Table 2. In the table, they are also compared with experiments when available. The differences between calculated parameters and experiments are comparable to the typical relative differences between calculations and experiments in complex oxides when using B3LYP functionals [36]. A similar underestimation of the calculated volume has been obtained for $\text{Zn}_2\text{V}_2\text{O}_7$ [28] and $\text{Cd}_2\text{V}_2\text{O}_7$ [29] using B3LYP functionals [32–34].

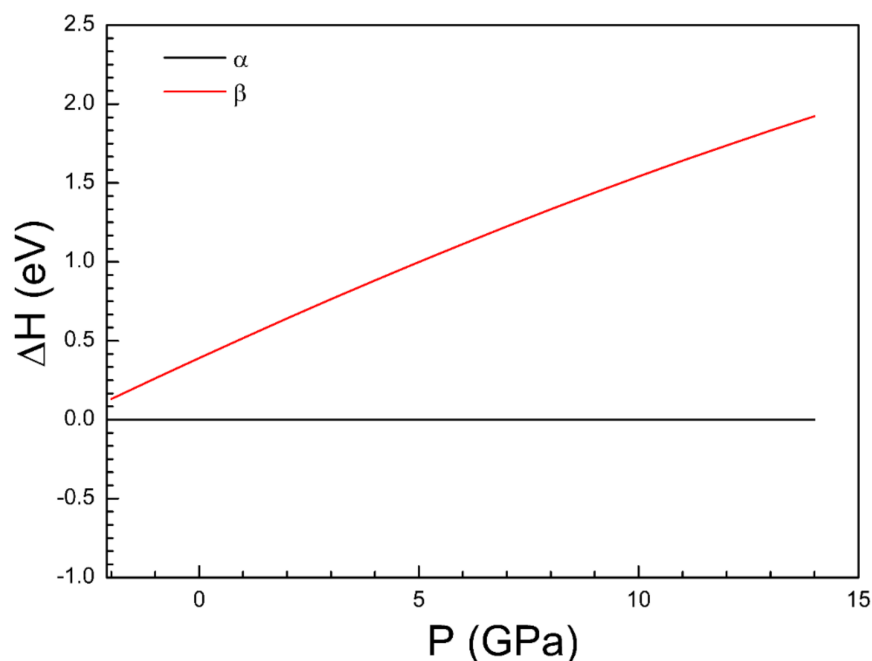


Figure 2. Calculated enthalpy difference versus pressure between the α -phase and β -phase of $\text{Cd}_3\text{V}_2\text{O}_8$ using α - $\text{Cd}_3\text{V}_2\text{O}_8$ as reference. The enthalpy of α - $\text{Cd}_3\text{V}_2\text{O}_8$ (black line) is the lowest in the complete pressure range.

Table 1. Calculated atomic positions of α - $\text{Cd}_3\text{V}_2\text{O}_8$.

Atom	Site	x	y	z
Cd ₁	4a	0	0	0
Cd ₂	8e	0.25	0.1554	0.25
V ₁	8f	0	0.3902	0.1247
O ₁	8f	0	0.2784	0.2491
O ₂	8g	0	0.0121	0.247
O ₃	16g	0.2134	0.3815	0.9847

Table 2. Unit-cell parameters and volume of different orthovanadates at zero pressure calculated with B3LYP functionals. They are compared with experiments [32–34]. The last column is the relative difference between calculations and experiments (ϵ) in %.

α -Cd ₃ V ₂ O ₈	B3LYP		
a (Å)	6.5837		
b (Å)	11.9604		
c (Å)	8.5473		
V (Å ³)	673.046		
β -Cd ₃ V ₂ O ₈	B3LYP	Exp. [34]	ϵ(%)
a (Å)	6.8744	6.9882	−1.6
b (Å)	5.3107	5.3251	−0.3
c (Å)	9.7796	9.8133	−0.3
V (Å ³)	357.032	365.18	−2.2
Zn ₃ V ₂ O ₈	B3LYP	Exp. [32]	ϵ(%)
a (Å)	6.0332	6.088	−0.9
b (Å)	11.4247	11.489	−0.6
c (Å)	8.1709	8.280	−1.3
V (Å ³)	563.200	579.145	−2.8
Mg ₃ V ₂ O ₈	B3LYP	Exp. [33]	ϵ(%)
a (Å)	5.9061	6.053	−2.4
b (Å)	11.2516	11.442	−1.7
c (Å)	8.1216	8.33	−2.5
V (Å ³)	539.705	576.923	−6.4
Ni ₃ V ₂ O ₈	B3LYP	Exp. [34]	ϵ(%)
a (Å)	5.685	5.936	−4.2
b (Å)	11.4508	11.42	−0.3
c (Å)	8.1093	8.24	−1.5
V (Å ³)	527.903	558.582	−5.5

In Table 3, we have summarized the optimized unit-cell volume at zero pressure obtained using HSE06 and PBE functionals. The comparison of results in Tables 2 and 3 supports that the B3LYP functionals describe orthovanadates more accurately than the other two functionals we have tested. If our results are compared with results reported in the Materials Project [37], which have been obtained using VASP [38,39] and PBE functionals, it can be also seen that B3LYP implemented in CRYSTAL14 gives the most precise description of the studied compounds. In particular, the VASP calculations systematically overestimate the volume at zero pressure.

Table 3. Volume of studied compounds calculated with HSE06 and PBE functionals. The relative difference between calculations and experiments (ϵ) is also given. Results from the Materials Project (MP) are also included.

Compound	V _{HSE06} (Å ³)	V _{PBE} (Å ³)	ϵ _{HSE06} (%)	ϵ _{PBE} (%)	V _{MP} (Å ³)	ϵ _{MP} (%)
α -Cd ₃ V ₂ O ₈	656.413	669.242				
β -Cd ₃ V ₂ O ₈	348.866	355.061	−4.5	−2.8	384.85	5.4
Zn ₃ V ₂ O ₈	549.367	559.630	−5.1	−3.4	609.12	5.2
Mg ₃ V ₂ O ₈	530.461	541.487	−8.1	−6.1	599.51	3.9
Ni ₃ V ₂ O ₈	503.762	504.320	−9.8	−8.7	579.38	3.7

3.2. Pressure–Volume Equation of State and Compressibility

Now we will comment the evolution of the unit-cell parameters of all compounds. In Figure 3, we represent the pressure dependence of unit-cell parameters. From these results, we have determined the linear compressibility coefficients ($k_l = -\frac{1}{l} \frac{\partial l}{\partial P}$), which are summarized in Table 4. Notice that all compounds described by space group *Cmca* show a similar anisotropy. In the four compounds, we found that $k_a > k_c > k_b$. In the case of $\text{Ni}_3\text{V}_2\text{O}_8$ and $\text{Zn}_3\text{V}_2\text{O}_8$, the results from calculations agree with experiments [14,15]. In the case of $\beta\text{-Cd}_3\text{V}_2\text{O}_8$, the response to compression is also anisotropic, being also the material which is considerably more compressible along the *a*-axis than along the perpendicular directions.

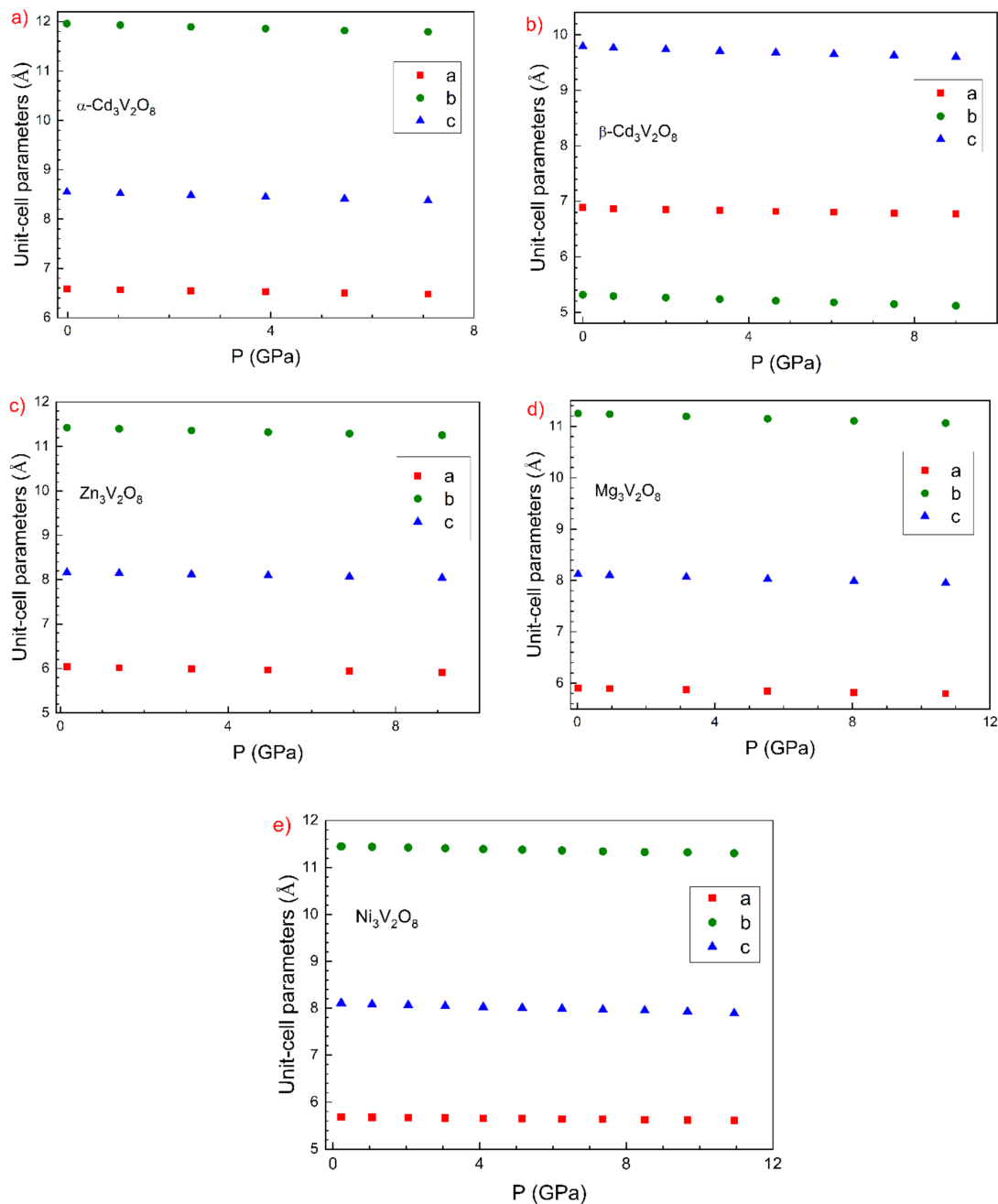


Figure 3. Calculated pressure dependence of the unit-cell parameters of different studied compounds. (a) $\alpha\text{-Cd}_3\text{V}_2\text{O}_8$, (b) $\beta\text{-Cd}_3\text{V}_2\text{O}_8$, (c) $\text{Zn}_3\text{V}_2\text{O}_8$, (d) $\text{Mg}_3\text{V}_2\text{O}_8$, and (e) $\text{Ni}_3\text{V}_2\text{O}_8$. The different unit-cell parameters are identified in the figures.

Table 4. Calculated linear compressibility coefficients of different compounds compared with experiments [14,15].

α -Cd ₃ V ₂ O ₈	$k_a = 2.73(4)10^{-3}$ GPa ⁻¹ $k_b = 1.76(6)10^{-3}$ GPa ⁻¹ $k_c = 2.27(11)10^{-3}$ GPa ⁻¹	
β -Cd ₃ V ₂ O ₈	$k_a = 4.16(4)10^{-3}$ GPa ⁻¹ $k_b = 1.88(1)10^{-3}$ GPa ⁻¹ $k_c = 1.56(3)10^{-3}$ GPa ⁻¹	
Zn ₃ V ₂ O ₈	$k_a = 2.31(3)10^{-3}$ GPa ⁻¹ $k_b = 1.59(2)10^{-3}$ GPa ⁻¹ $k_c = 2.24(3)10^{-3}$ GPa ⁻¹	$k_a = 2.9(1)10^{-3}$ GPa ⁻¹ [14] $k_b = 1.9(1)10^{-3}$ GPa ⁻¹ $k_c = 2.7(1)10^{-3}$ GPa ⁻¹
Mg ₃ V ₂ O ₈	$k_a = 2.59(1)10^{-3}$ GPa ⁻¹ $k_b = 1.59(1)10^{-3}$ GPa ⁻¹ $k_c = 2.37(1)10^{-3}$ GPa ⁻¹	
Ni ₃ V ₂ O ₈	$k_a = 2.89(51)10^{-3}$ GPa ⁻¹ $k_b = 1.46(4)10^{-3}$ GPa ⁻¹ $k_c = 2.33(3)10^{-3}$ GPa ⁻¹	$k_a = 2.7(1)10^{-3}$ GPa ⁻¹ [15] $k_b = 1.79(6)10^{-3}$ GPa ⁻¹ $k_c = 2.33(5)10^{-3}$ GPa ⁻¹

In the case of the four isomorphous compounds (those described by space group *Cmca*), the observed anisotropy is related to the layered nature of the Kagome-type structure. For these materials, it can be assumed that pressure-induced changes in the crystal structure are mainly determined by changes in the octahedral units [40,41]. This is because the VO₄ tetrahedron, due to the strong V 3*d*-O 2*p* hybridization [40], behaves as a rigid unit and changes little under compression [41]. As can be seen in Figure 1a, the crystal structure of these orthovanadates contains two-dimensional Kagome ladders of compressible MO₆ octahedral units. These octahedral chains form compressible layers that lie perpendicular to the *b*-axis of the structure. These layers are separated by the less compressible VO₄ tetrahedra, which are arranged to form pillars between them, reducing the compressibility along the *b*-axis and making it the least compressible axis. A similar picture can be used to explain the anisotropy of β -Cd₃V₂O₈. In this polymorph, there are linear chains of CdO₆ octahedra aligned along the *a*-axis. The layers are connected by corner-sharing VO₄ tetrahedra. These characteristics make the *a*-axis the easiest direction of compression.

The calculated pressure dependence of the unit-cell volume is shown in Figure 4. We have fitted these results using a third-order Birch–Murnaghan equation of state [42] for each of the studied compounds. From the fits, we have obtained the zero-pressure unit-cell volume [*V*₀], bulk modulus [*K*₀], and its pressure derivative [*K*₀′]. We summarize the values obtained for these parameters in Table 5. The fittings have been carried out using the program Eosfit [43]. We have found that there is a tendency to a decrease in *K*₀ as *V*₀ increases. This is a consequence of the increase in the packing efficiency as the volume is reduced. In addition, we have noticed that in the cases of Ni₃V₂O₈ and Zn₃V₂O₈ (the two compounds for which experimental results are available), our results systematically underestimate the experimental compressibility (see Figure 4), which leads to an overestimation of the bulk modulus by approximately 20 GPa [14,15]. This is consistent with the fact that our calculations underestimate *V*₀. Notice that both parameters are correlated and an underestimated *V*₀ will always lead to an overestimated *B*₀ [44,45]. Both facts can be a consequence of an overestimation of the interactions between atoms, which can cause over-hybridization of the M–O bonds because of a self-interaction error [46].

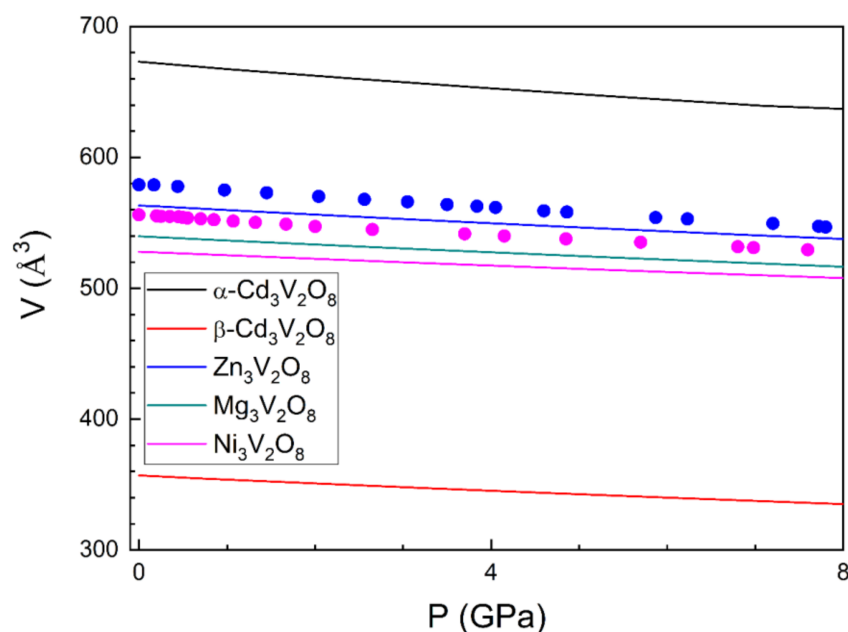


Figure 4. Pressure dependence of the unit-cell volume for different compounds. Solid lines are the results of calculations. Circles are results from previous experiments [14,15].

Table 5. The unit-cell volume (\AA^3), bulk modulus (GPa), and bulk modulus pressure derivative at ambient pressure determined using a third-order Birch–Murnaghan EOS.

Phase	$V_0 (\text{\AA}^3)$	$K (\text{GPa})$	K'_0
$\alpha\text{-Cd}_3\text{V}_2\text{O}_8$	673.0	112	5.0
$\beta\text{-Cd}_3\text{V}_2\text{O}_8$	357.0	92	4.0
$\text{Zn}_3\text{V}_2\text{O}_8$	563.2	136	5.4
$\text{Mg}_3\text{V}_2\text{O}_8$	539.7	146	4.4
$\text{Ni}_3\text{V}_2\text{O}_8$	527.9	171	4.5

To further understand the changes in the unit-cell volume of the studied compounds under compression, we have analysed changes in polyhedral volumes with pressure. In Figure 5, we report relative changes in the unit-cell volume and relative changes in the polyhedral volumes for each compound. In the figure, it can be seen that, in all compounds, most of the volume change is accounted for by the compression of the MO_6 octahedra. This observation supports the hypothesis we used to explain the anisotropy of the compressibility. In particular, in $\text{Mg}_3\text{V}_2\text{O}_8$ and $\text{Zn}_3\text{V}_2\text{O}_8$, it is quite notorious that the relative compressibility of MgO_6 and ZnO_6 is comparable to that of the respective compounds. In the other three cases, the contribution of the volume change in VO_4 is less negligible than in $\text{Mg}_3\text{V}_2\text{O}_8$ and $\text{Zn}_3\text{V}_2\text{O}_8$.

On the other hand, our findings also agree with the conclusions extracted by Hazen et al. [47] from the analysis of multiple ternary oxides. These authors established that the bulk modulus of ternary oxides is determined by the compressibility of the largest polyhedra. They proposed that the bulk modulus is expected to have a linear dependence with the average volume of the larger cation polyhedron multiplied by the cation formal charge. In our cases, this means that K_0 is proportional to Z/d^3 , where $Z = 2$ is the formal charge of divalent M cation, and d is the average M–O bond distance within the MO_6 octahedron. In Figure 6, we plot our calculated K_0 versus Z/d^3 . In the figure, we also include available experimental results [15,16]. Results from $\text{Cu}_3\text{V}_2\text{O}_8$ have been excluded, because it has a very different crystal structure where part of the Cu atoms are in highly unusual square-planar geometry [48]. As a consequence, this compound is extremely unstable under HP, decomposing into $3\text{CuO} + \text{V}_2\text{O}_5$. In Figure 6, it can be seen that in spite

of the offset between experiments and calculations, both sets of results follow the expected linear dependence, confirming that the changes induced in the structure by pressure are mainly due to changes in MO_6 octahedral units.

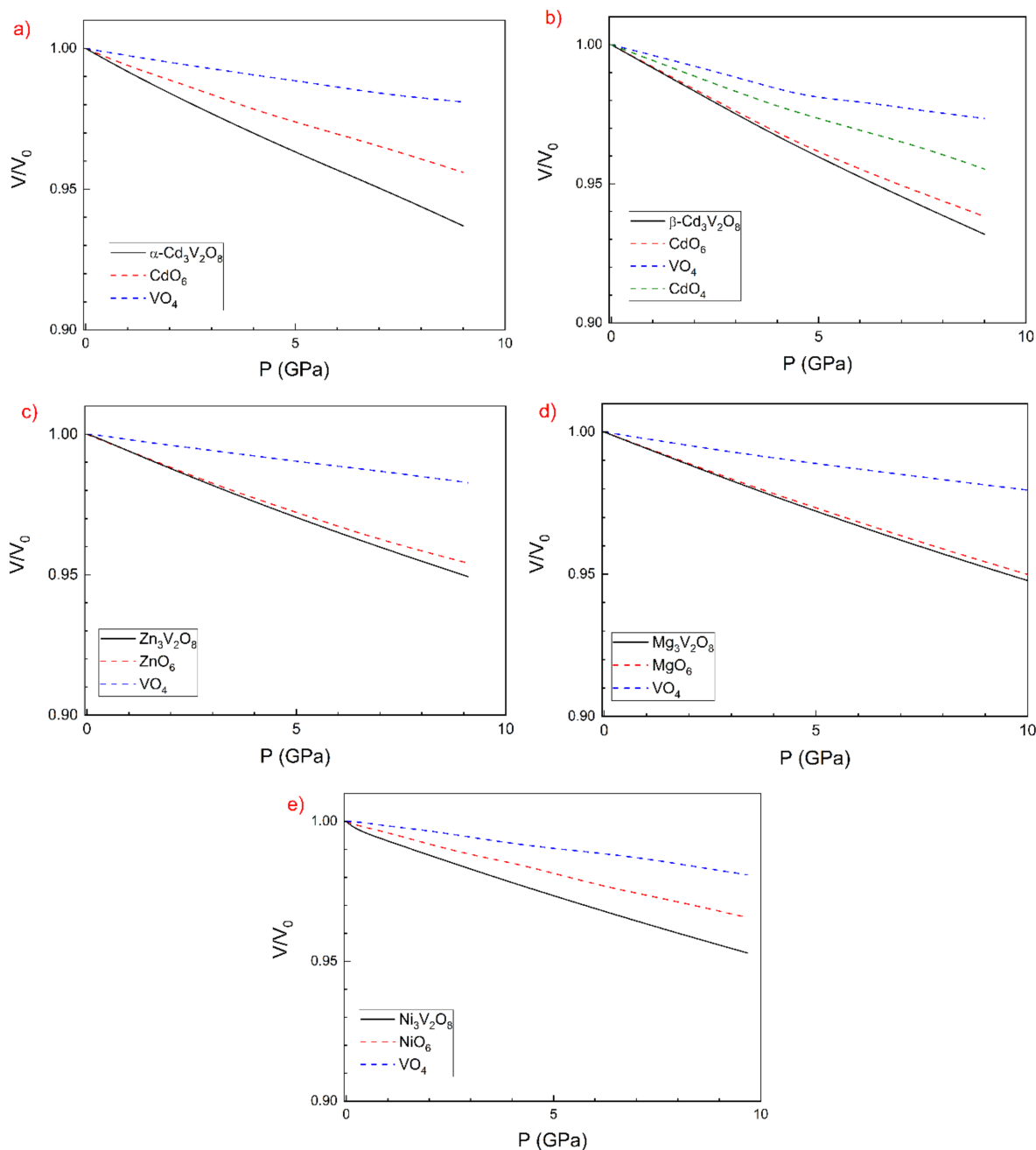


Figure 5. Evolution with the normalized volume relative to the zero-pressure volume and evolution of the relative volume of polyhedral units.

In addition to the bulk modulus, the hardness, a measure of the resistance to localized plastic deformation, is a very important physical parameter for technological applications, in particular for using $\text{M}_3\text{V}_2\text{O}_8$ as laser-host materials. To the best of our knowledge, their hardness is unknown. We have estimated it from the calculated bulk moduli using the relation proposed by She et al. [49]. We have obtained that the hardness goes from 12(2) GPa in $\text{Cd}_3\text{V}_2\text{O}_8$ to 20(2) GPa in $\text{Ni}_3\text{V}_2\text{O}_8$. These values are similar to the values previously reported for zircon-type orthovanadates [50].

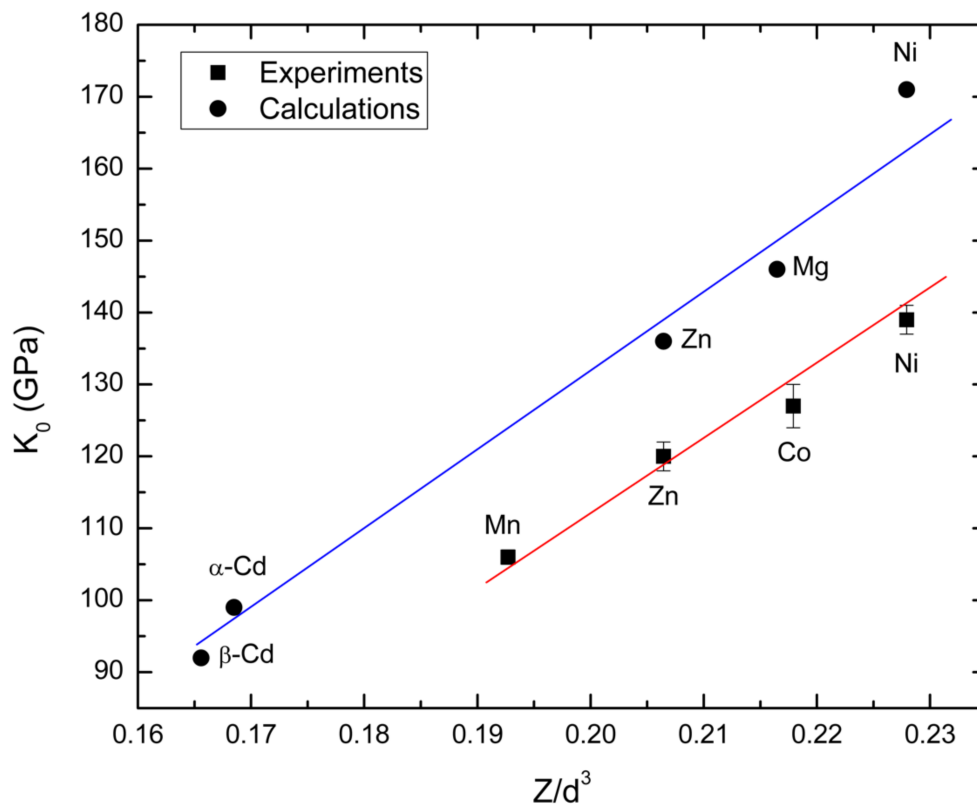


Figure 6. Values of the theoretical ambient-pressure bulk modulus (K_0) of studied orthovanadates versus the cation charge density of the MO_6 octahedron (Z/d^3). Squares represent experimental results and circles the results from present calculations. The solid lines are a guide to the eyes.

4. Conclusions

In this work, we have studied and compared the compressibility behavior under pressure of four different metal orthovanadates using density-functional theory calculations. We have determined that B3LYP functionals describe better than HSE06 and PBE functionals the crystal structure of $\text{Cd}_3\text{V}_2\text{O}_8$, $\text{Zn}_3\text{V}_2\text{O}_8$, $\text{Mg}_3\text{V}_2\text{O}_8$, and $\text{Ni}_3\text{V}_2\text{O}_8$. In $\text{Cd}_3\text{V}_2\text{O}_8$, we have also discovered a new polymorph which is thermodynamically more favorable than the previously known polymorph. In addition, we have determined the pressure dependence of unit-cell parameters. The compressibility of the different compounds is anisotropic. For the different materials, the anisotropy has been discussed in detail, being the principal compression axis determined. We have also determined a pressure–volume equation of states from which the bulk moduli have been obtained. This magnitude has been related to changes in the volume of the divalent cation coordination octahedra. The comparison of the compounds allowed us to verify that their bulk modulus can be explained using the model proposed by Hazen et al. for ternary oxides.

Author Contributions: Conceptualization, D.E.; computer simulations, D.D.-A.; analysis, D.E. and D.D.-A.; writing—review and editing, both authors. All authors have read and agreed to the published version of the manuscript.

Funding: D.E. thanks the financial support from Generalitat Valenciana under Grant PROMETEO CIPROM/2021/075-GREENMAT and MFA/2022/007 and by the Spanish Research Agency (AEI) and Spanish Ministry of Science and Investigation (MCIN) under projects PID2019-106383GB-C41 (DOI: 10.13039/501100011033) and RED2018-102612-T (MALTA Consolider-Team Network). D.D.-A. acknowledges the PhD fellowship granted by Generalitat Valencia (ACIF/2020/009).

Acknowledgments: The authors thank MALTA supercomputer for providing the tools for theoretical calculations.

Conflicts of Interest: The authors declare no conflict of interest.

References

1. Liu, H.; Cui, Y. Microwave-assisted hydrothermal synthesis of hollow flower-like $Zn_2V_2O_7$ with enhanced cycling stability as electrode for lithium ion batteries. *Mater. Lett.* **2018**, *228*, 369–371. [CrossRef]
2. Sameie, H.; Sabbagh Alvani, A.A.; Naseri, N.; Du, S.; Rosei, F. First-principles study on ZnV_2O_6 and $Zn_2V_2O_7$: Two new photoanode candidates for photoelectrochemical water oxidation. *Ceram. Int.* **2018**, *44*, 6607–6613. [CrossRef]
3. Bayat, A.; Mahjoub, A.R.; Amini, M.M. Optical properties of hydrophilic surfaced self-assembled $Cd_2V_2O_7$ hollow sphere shape architecture. *Mater. Lett.* **2016**, *186*, 252–255. [CrossRef]
4. Zhi, J. Study of MgV_2O_6 as Cathode Material for Secondary Magnesium Batteries. *Asian J. Chem.* **2011**, *23*, 1399–1400.
5. Ni, S.; Liu, J.; Chao, D.; Mai, L. Vanadate-Based Materials for Li-Ion Batteries: The Search for Anodes for Practical Applications. *Adv. Energy Mater.* **2019**, *9*, 1803324. [CrossRef]
6. Hassan, A.; Iqbal, T.; Tahir, M.B.; Afsheen, S. A review on copper vanadate-based nanostructures for photocatalysis energy production. *Int. J. Energy Res.* **2019**, *43*, 9–28. [CrossRef]
7. Vijayakumar, S.; Lee, S.-H.; Ryu, K.-S. Synthesis of $Zn_3V_2O_8$ nanoplatelets for lithium-ion battery and supercapacitor applications. *RSC Adv.* **2015**, *5*, 91822–91828. [CrossRef]
8. Cabrera, I.; Kenzelmann, M.; Lawes, G.; Chen, Y.; Chen, W.; Erwin, R.; Gentile, T.R.; Leao, J.B.; Lynn, J.W.; Rogado, N.; et al. Coupled Magnetic and Ferroelectric Domains in Multiferroic $Ni_3V_2O_8$. *Phys. Rev. Lett.* **2009**, *103*, 087201. [CrossRef]
9. Birdeanu, M.-I.; Vaida, M.; Ursu, D.; Fagadar-Cosma, E. Obtaining and characterization of $Zn_3V_2O_8$ and $Mg_3V_2O_8$ pseudo binary oxide nanomaterials by hydrothermal method. In *High Energy Gamma-Ray Astronomy, Proceedings of the 6th International Meeting on High-Energy Gamma-Ray Astronomy, Heidelberg, Germany, 11–15 July 2016*; AIP Publishing LLC: Melville, NY, USA, 2017; p. 030006.
10. Mazloom, F.; Masjedi-Arani, M.; Salavati-Niasari, M. Novel size-controlled fabrication of pure $Zn_3V_2O_8$ nanostructures via a simple precipitation approach. *J. Mater. Sci. Mater. Electron.* **2015**, *27*, 1974–1982. [CrossRef]
11. Luo, J.; Chen, R.; Zhang, X. The Effect in the Production and Luminescence Property of $Zn_3V_2O_8$ with Eu-doping and the First Principle Calculation of α - $Zn_3V_2O_8$. *Mater. Sci. Eng.* **2017**, *274*, 012087. [CrossRef]
12. Qian, T.; Fan, B.; Wang, H.; Zhu, S. Structure and luminescence properties of $Zn_3V_2O_8$ yellow phosphor for white light emitting diodes. *Chem. Phys. Lett.* **2019**, *715*, 34–39. [CrossRef]
13. Matsushima, Y.; Koide, T.; Hiro-Oka, M.; Shida, M.; Sato, A.; Sugiyama, S.; Ito, M. Self-activated vanadate compounds toward realization of rare-earth-free full-color phosphors. *J. Am. Ceram. Soc.* **2015**, *98*, 1236–1244. [CrossRef]
14. Díaz-Anichtchenko, D.; Santamaria-Perez, D.; Marqueño, T.; Pellicer-Porres, J.; Ruiz-Fuertes, J.; Ribes, R.; Errandonea, D. Comparative study of the high-pressure behavior of ZnV_2O_6 , $Zn_2V_2O_7$, and $Zn_3V_2O_8$. *J. Alloys Compd.* **2020**, *837*, 155505. [CrossRef]
15. Díaz-Anichtchenko, D.; Turnbull, R.; Bandiello, E.; Anzellini, S.; Errandonea, D. High-Pressure Structural Behavior and Equation of State of Kagome Staircase Compound, $Ni_3V_2O_8$. *Crystals* **2020**, *10*, 910. [CrossRef]
16. Kesari, S.; Garg, A.B.; Clemens, O.; Joseph, B.; Rao, R. Pressure-Induced Structural Behavior of Orthorhombic $Mn_3(VO_4)_2$: Raman Spectroscopic and X-ray Diffraction Investigations. *ACS Omega* **2022**, *7*, 3099–3108. [CrossRef]
17. Beltrán, A.; Gracia, L.; Andrés, J. Polymorphs of ZnV_2O_6 under pressure: A first-principle investigation. *J. Phys. Chem. C* **2019**, *123*, 3239–3253. [CrossRef]
18. Lopez-Moreno, S.; Errandonea, D.; Rodriguez-Hernandez, P.; Munoz, A. Polymorphs of $CaSeO_4$ under pressure: A first-principles study of structural, electronic, and vibrational properties. *Inorg. Chem.* **2015**, *54*, 1765–1777. [CrossRef]
19. Benmakhlouf, A.; Errandonea, D.; Bouchenafa, M.; Maabed, S.; Bouhemadou, A.; Bentabet, A. New pressure-induced polymorphic transitions of anhydrous magnesium sulfate. *Dalton Trans.* **2017**, *46*, 5058–5068. [CrossRef]
20. Errandonea, D.; Gracia, L.; Lacomba-Perales, R.; Polian, A.; Chervin, J.C. Compression of scheelite-type $SrMoO_4$ under quasi-hydrostatic conditions: Redefining the high-pressure structural sequence. *J. Appl. Phys.* **2013**, *113*, 123510. [CrossRef]
21. Dovesi, R.; Saunders, V.R.; Roetti, C.; Orlando, R.; Zicovich-Wilson, C.M.; Pascale, F.; Civalieri, B.; Doll, K.; Harrison, N.M.; Bush, I.J.; et al. *CRYSTAL14 User's Manual*; University of Torino: Torino, Italy, 2014.
22. Becke, A.D. Density-functional thermochemistry. III. The role of exact exchange. *J. Chem. Phys.* **1993**, *98*, 5648–5652. [CrossRef]
23. Lee, C.; Yang, W.; Parr, R.G. Development of the Colle-Salvetti correlation-energy formula into a functional of the electron density. *Phys. Rev. B* **1988**, *37*, 785–789. [CrossRef] [PubMed]
24. Heyd, J.; Scuseria, G.E.; Ernzerhof, M.E. Hybrid functionals based on a screened Coulomb potential. *J. Chem. Phys.* **2003**, *118*, 8207–8215. [CrossRef]
25. Perdew, J.P.; Wang, Y. Accurate and simple analytic representation of the electron-gas correlation energy. *Phys. Rev. B* **1992**, *45*, 13244–13249. [CrossRef] [PubMed]
26. Available online: <http://www.crystal.unito.it/basis-sets.php/> (accessed on 14 October 2022).
27. Freysoldt, C.; Grabowski, B.; Hickel, T.; Neugebauer, J.; Kresse, G.; Janotti, A.; van de Walle, C.G. First-principles calculations for point defects in solids. *Rev. Mod. Phys.* **2014**, *86*, 253–305. [CrossRef]
28. Díaz-Anichtchenko, D.; Gracia, L.; Errandonea, D. Density-functional study of pressure-induced phase transitions and electronic properties of $Zn_2V_2O_7$. *RSC Adv.* **2021**, *11*, 10401–10415. [CrossRef] [PubMed]

29. Diaz-Anichtchenko, D.; Errandonea, D. Pressure-induced phase transitions and electronic properties of $\text{Cd}_2\text{V}_2\text{O}_7$. *RSC Adv.* **2022**, *12*, 14827–14837. [[CrossRef](#)]
30. Grimme, S. Semiempirical GGA-Type Density Functional Constructed with a Long-Range Dispersion Correction. *J. Comput. Chem.* **2006**, *27*, 1787–1799. [[CrossRef](#)]
31. Momma, K.; Izumi, F. VESTA 3 for Three-Dimensional Visualization of Crystal, Volumetric and Morphology Data. *J. Appl. Crystallogr.* **2011**, *44*, 1272–1276. [[CrossRef](#)]
32. Gopal, R.; Calvo, C. Crystal structure of $\alpha\text{-Zn}_3\text{V}_2\text{O}_8$. *Can. J. Chem.* **1971**, *49*, 3056–3059. [[CrossRef](#)]
33. Krishnamachari, N.; Calvo, C. Refinement of the Structure of $\text{Mg}_3\text{V}_2\text{O}_8$. *Can. J. Chem.* **1971**, *49*, 1629–1637. [[CrossRef](#)]
34. Saurbrei, E.E.; Faggiani, R.; Calvo, C. Refinement of the Crystal structures of $\text{Cd}_3\text{V}_2\text{O}_8$ and $\text{Ni}_3\text{V}_2\text{O}_8$. *Acta Cryst.* **1973**, *B29*, 2304–2306. [[CrossRef](#)]
35. Yahia, H.B.; Gaudin, E.; Feral-Martin, C.; Darriet, J. Structural study of the $\text{NaCdVO}_4\text{-Cd}_3\text{V}_2\text{O}_8$ and $\text{CdO-V}_2\text{O}_5$ sections of the ternary system $\text{Na}_2\text{O-CdO-V}_2\text{O}_5$. *J. Solid State Chem.* **2010**, *183*, 776–783. [[CrossRef](#)]
36. Burke, K. Perspective on density functional theory. *J. Chem. Phys.* **2012**, *136*, 150901. [[CrossRef](#)]
37. Available online: <https://materialsproject.org/> (accessed on 14 October 2022).
38. Kresse, G.; Furthmüller, J. Efficiency of Ab-Initio Total Energy Calculations for Metals and Semiconductors Using a Plane-Wave Basis Set. *Comput. Mater. Sci.* **1996**, *6*, 15–50. [[CrossRef](#)]
39. Kresse, G.; Furthmüller, J. Efficient Iterative Schemes for Ab Initio Total-Energy Calculations Using a Plane-Wave Basis Set. *Phys. Rev. B* **1996**, *54*, 11169–11186. [[CrossRef](#)]
40. Laverock, J.; Piper, L.F.J.; Preston, A.R.H.; Chen, B.; McNulty, J.; Smith, K.E.; Guo, J.H. Strain dependence of bonding and hybridization across the metal-insulator transition of VO_2 . *Phys. Rev. B* **2012**, *85*, 081104. [[CrossRef](#)]
41. Errandonea, D. High pressure crystal structures of orthovanadates and their properties. *J. Appl. Phys.* **2020**, *128*, 040903. [[CrossRef](#)]
42. Birch, F. Finite elastic strain of cubic crystals. *Phys. Rev.* **1947**, *71*, 809. [[CrossRef](#)]
43. Gonzalez-Platas, J.; Alvaro, M.; Nestola, F.; Angel, R.J. EosFit7-GUI: A new GUI tool for equation of state calculations, analyses and teaching. *J. Appl. Cryst.* **2016**, *49*, 1377–1382. [[CrossRef](#)]
44. Anzellini, S.; Burakovsky, L.; Turnbull, R.; Bandiello, E.; Errandonea, D. P–V–T Equation of State of Iridium Up to 80 GPa and 3100 K. *Crystals* **2021**, *11*, 452. [[CrossRef](#)]
45. Angel, R.J. Equations of state. *Rev. Mineral. Geochem.* **2000**, *41*, 35–59. [[CrossRef](#)]
46. Piskunov, S.; Heifets, E.; Eglitis, R.I.; Borstel, G. Bulk properties and electronic structure of SrTiO_3 , BaTiO_3 , PbTiO_3 perovskites: An ab initio HF/DFT study. *Comput. Mater. Sci.* **2004**, *29*, 165–178. [[CrossRef](#)]
47. Errandonea, D.; Manjon, F.J. Pressure effects on the structural and electronic properties of ABX_4 scintillating crystals. *Prog. Mater. Sci.* **1997**, *53*, 711–773. [[CrossRef](#)]
48. Díaz-Anichtchenko, D.; Turnbull, R.; Bandiello, E.; Anzellini, S.; Achary, S.N.; Errandonea, D. Pressure-induced chemical decomposition of copper orthovanadate ($\alpha\text{-Cu}_3\text{V}_2\text{O}_8$). *J. Mater. Chem. C* **2021**, *9*, 13402–13409. [[CrossRef](#)]
49. She, J.; Sawamura, S.; Wondraczek, L. Scratch hardness of rare-earth substituted calcium aluminosilicate glasses. *J. Non-Cryst. Solids* **2019**, *1*, 100010. [[CrossRef](#)]
50. Huang, Z.; Feng, J.; Pan, W. Theoretical investigations of the physical properties of zircon-type YVO_4 . *J. Solid State Chem.* **2012**, *185*, 42–48. [[CrossRef](#)]